communications earth & environment

Article

https://doi.org/10.1038/s43247-024-01891-w

Impacts of agriculture and snow dynamics on catchment water balance in the U.S. and Great Britain

Masoud Zaerpour[1] ✉, Shadi Hatami[1], André S. Ballarin[2], Wouter J. M. Knoben[1], Simon Michael Papalexiou[1,3], Alain Pietroniro[1] & Martyn P. Clark[1]

The Budyko water balance is a fundamental concept in hydrology that links aridity to how precipitation is divided between evapotranspiration and streamflow. While the model is powerful, its ability to explain temporal changes and the influence of human activities and climate change is limited. Here we introduce a causal discovery algorithm to explore deviations from the Budyko water balance, attributing them to human interventions such as agricultural activities and snow dynamics. Our analysis of 1342 catchments across the U.S. and Great Britain reveals distinct patterns: in the U.S., snow fraction and irrigation alter the Budyko water balance predominantly through changes in aridity-streamflow relationships, while in Great Britain, deviations are primarily driven by changes in precipitation-streamflow relationships, notable in catchments with high cropland percentage. By integrating causal analysis with the Budyko water balance, we enhance understanding of how human activities and climate dynamics affect water balance, offering insights for water management and sustainability in the Anthropocene.

The water-energy balance is a cornerstone concept in hydrology, encapsulating the intricate interplay between water and energy fluxes within a catchment[1]. Understanding this balance is critical, as it governs the partitioning of precipitation (P) into evapotranspiration (E) and streamflow (Q)[2,3]. The equilibrium between incoming precipitation and the energy available for evaporation underpins the hydrological cycle, influencing water availability, ecosystem health, and human water use[4]. However, the catchment water balance is not static; the distribution is uneven across Earth's surface, driven by climatic patterns and human activities. Recognizing the factors that disrupt the catchment water balance is essential for managing water resources sustainably and mitigating the impacts of climate change and anthropogenic pressures on hydrological systems[5–9].

Central to the study of the water-energy balance is the Budyko curve[10], a framework that describes the relationship between climate aridity and the partitioning of P into E and Q (hereafter, when we mention the water-energy balance, we are referring to the equilibrium estimated by the Budyko curve —See Fig. 1a). Developed in the mid-20th century, the Budyko curve provides a simple and powerful tool to predict the long-term average behavior of catchments under varying climatic conditions[11–14]. According to the Budyko curve, the proportion of precipitation that evaporates versus contributes to streamflow is primarily determined by the dryness index (φ), a ratio of potential evapotranspiration to precipitation. This framework offers a valuable tool for comparing normalized observations across a wide spectrum of climatic conditions, enabling the identification of secondary controls on a catchment's water balance[13,15].

While the Budyko curve has been instrumental in advancing our understanding of catchment hydrology[11,16–18], it has some limitations[19]. Many Budyko-based studies often rely on temporal averages over multiple years to assess dominant controls of catchment water partitioning[11,16–18,20], omitting a substantial amount of hydrological information and the interplay of various factors that could influence water balance at finer temporal scales[21]. This is particularly evident when considering elasticity analyses, which often assume E and Q follow the Budyko curve, though this assumption may be less accurate during the timeframes when a catchment establishes a new equilibrium[20,22]. Such limitations are particularly relevant when considering the significant influence of human activities, such as agriculture and irrigation, and climatic factors like snow fraction, which alter the water-energy balance and contribute to deviations from the Budyko curve's predictions. In fact, climate change and human activities lead to new prevailing conditions and cause deviations from the Budyko curve predictions[14,15,23–25]. These deviations underscore the need to refine our

[1]Department of Civil Engineering, Schulich School of Engineering, University of Calgary, Calgary, AB, Canada. [2]Department of Hydraulics and Sanitation, São Carlos School of Engineering, University of São Paulo, São Paulo, Brazil. [3]Faculty of Environmental Sciences, Czech University of Life Sciences, Prague, Czech Republic. ✉e-mail: masoud.zaerpour@ucalgary.ca

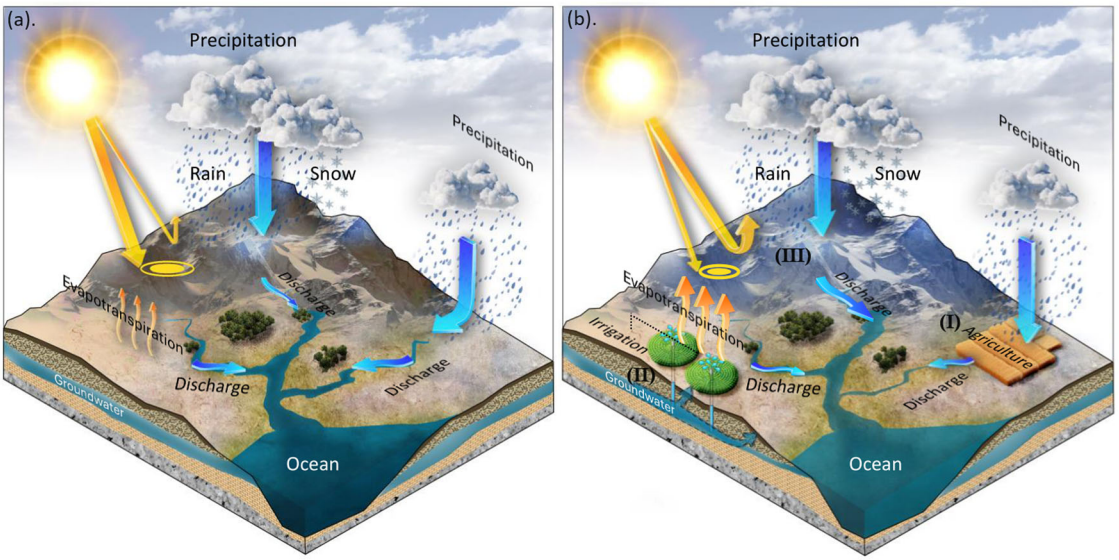

Fig. 1 | Schematic representation of water cycle changes. Schematic representation of changes in the water cycle. **a** a standard water-energy balance equilibrium as per the Budyko hypothesis. **b** the changes in the water-energy balance due to agriculture (I) irrigation (II), and changes in snow fraction (III).

models and approaches to account for climate change and anthropogenic influences on the water-energy balance, particularly at finer time scales.

Among human activities, agriculture, in particular, has a profound impact on the water-energy balance[26–28] (Fig. 1b, I). As the largest consumer of freshwater globally, agricultural practices account for approximately 72% of global water withdrawals[29], altering the natural flow and storage of water through agricultural crop expansion, irrigation, and land management[28,30]. The expansion of agricultural lands and the intensification of water use for irrigation modify the surface albedo, soil moisture, and vegetation cover, influencing evapotranspiration rates and the partitioning of precipitation[31]. Global estimates of water utilized for crops span from 2217 to 3185 km^3 per year[32,33], while additional crop evapotranspiration encompasses a range of 927–1530 km^3 per year[34]. Although agricultural expansion sustains food security, at the same time, it exacerbates water scarcity and affects downstream water availability[35,36]. The abstraction of water for agriculture/irrigation from surface and groundwater sources can lead to substantial alterations in water-energy balance (Fig. 1b, II). For example, the US Ogallala Aquifer has seen a dramatic groundwater extraction due to agricultural activities[37,38]. Hence, understanding the magnitude and mechanisms of agriculture's impact by water sources on the water-energy balance is crucial for developing strategies to mitigate its effects and ensure the sustainable management of water resources.

Changes in snow fraction, the proportion of precipitation falling as snow, also play a critical role in altering the water-energy balance[39] (Fig. 1b, III). Snow fraction acts as a temporary storage for precipitation, releasing water into the system through snowmelt at different times of the year[8,40]. This seasonal storage and release mechanism can influence the dynamics between precipitation, aridity, and streamflow. Research on streamflow elasticity in snowy catchments consistently demonstrates low elasticity values, indicating the buffering effect of snow on streamflow response to precipitation[41,42]. Additionally, changes in snow cover affect the energy balance through its albedo, reflecting a large portion of incoming solar radiation and thus influencing the timing and rate of snowmelt and evapotranspiration[2,43]. Studies show that a decrease in albedo due to climate change-induced snowmelt is particularly pronounced during the spring and autumn transition periods, leading to a significant increase in net shortwave solar radiation absorbed by the surface[44]. The decreased albedo due to a reduction of snow fraction results in an increase in evapotranspiration and thereby a decrease in streamflow[6,7,45].

A comprehensive understanding of the water-energy balance enhances our evaluation of freshwater resources and enables us to understand global water security threats more effectively. On a global scale, climate change has been identified as a primary driver of water-energy changes[46,47]. Nonetheless, at the regional scale the water-energy balance is not solely shaped by climate dynamics[9,48–50]; it is also influenced by other human interferences like agriculture[15,51,52]. Shifts within the Budyko space are associated with changes in climate such as snow-to-rain ratio[14,53] and distinct human activities, including the construction of reservoirs[54–56], forestry practices[57,58], agricultural expansion, and changes in land cover[15,59–61]. Despite the essential role of agriculture and climatic factors other than precipitation and evapotranspiration in shaping the hydrological cycle, assessing the global impact of all these factors remains challenging. This is due to the lack of a standardized approach to quantify the impact of several controlling variables at a fine temporal scale, uncertainties associated with factors such as agricultural area delineation, hydrological modelling, and critical local parameters, including soil hydraulic characteristics, and the relation of these factors to water availability[62].

To address these challenges, we combine the Budyko curve with a causal discovery algorithm[63,64] to enhance our understanding of the water-energy balance. By integrating the Budyko curve with the Peter–Clark Momentary Conditional Independence Plus (PCMCI+) causal algorithm[65,66], we aim to study how catchments deviate from the Budyko water-energy balance and what causes these deviations. Our approach initially examines deviations from the Budyko curve and their relationships to alterations in causal links among precipitation, aridity, and streamflow. Subsequently, our investigation focuses on factors disturbing the causal links. By examining the causal relationships between these components, we gain a deeper understanding of the dynamics shaping catchment hydrology and water availability.

In hydrometeorology, causality analysis is a burgeoning field in model simulations but is still rarely used in observational studies. To the best of our knowledge, this study offers a novel perspective on interpreting deviations from the Budyko curve equilibrium (i.e., causality) by focusing on observational data[67,68]. We employ the PCMCI+ algorithm[65,66,69]—a recent advancement in Earth System sciences—to systematically explore causal relationships among hydroclimatic variables. PCMCI+ integrates a variant of the PC algorithm with the momentary conditional independence (MCI) measure to identify both contemporaneous and time-lagged causal links in high-dimensional, autocorrelated time series. Unlike correlation analysis, PCMCI+ can exclude dependencies caused by common drivers or indirect paths through conditional independence tests.

By applying PCMCI+ to an extensive dataset of catchments, this study uncovers the impacts of agriculture and snow fraction on the water-energy balance, enhancing our understanding of hydrological processes. It also

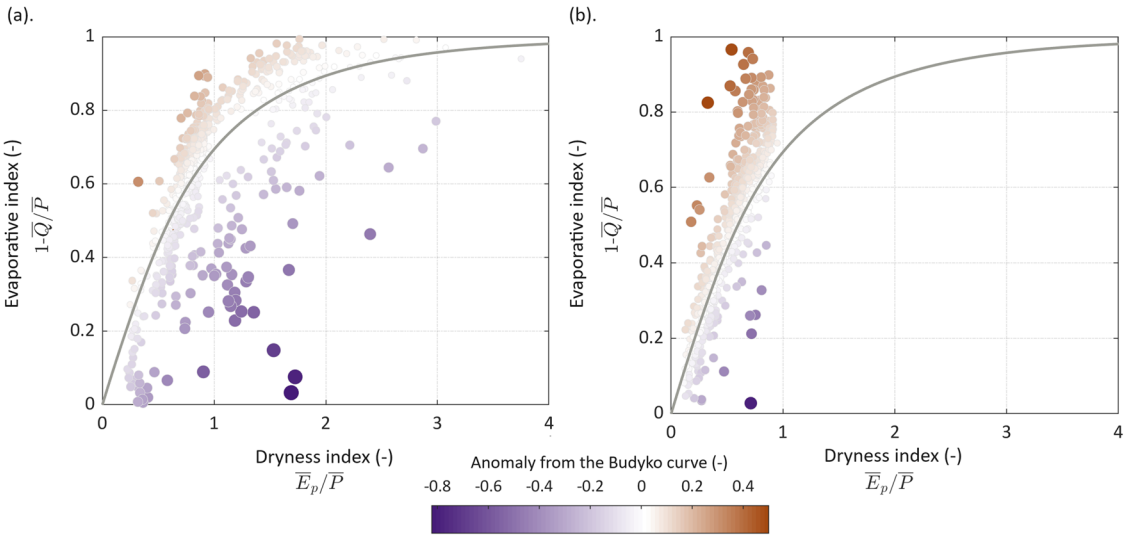

Fig. 2 | Long-term observed data of studied catchments within the Budyko framework. The long-term observed data are placed within the framework of the Budyko hypothesis for the US and GB datasets, as depicted in (**a**, **b**), respectively (See Method section for further information on the equations that were used). The colours indicate the distance from the Budyko curve.

provides a framework for predicting the effects of future climatic and anthropogenic changes on water resources. Our analysis focuses on 1342 Catchment Attributes and Meteorology for Large-sample Studies (CAMELS) catchments located across the contiguous United States (US) and Great Britain (GB) from 1980 to 2014. We investigate the role of agriculture by a spatial (between-catchment) comparison of the long-term partitioning of precipitation into evaporation and streamflow due to the lack of CL% time series. We also examine alterations in the strength of causal links and its relation to snow fraction and/or the cropland percentage (CL%; as an agriculture proxy), shedding light on the effect of these factors on altering the water-energy balance. For this purpose, we analyze temporal changes of individual responses at the seasonal time scale[20,22]. Our examination focuses on three key factors influencing streamflow (Q): precipitation (P), aridity (AR), and snow fraction (SF)[20,70,71]. This approach allows for an investigation into how various components influence water partitioning by examining the water-energy balance from a new perspective—focusing on the equilibrium between water and energy components, which has not been previously explored.

Results

The long-term observations of 671 US catchments within the context of the Budyko hypothesis[10] are shown in Fig. 2a. Overall, the average absolute deviation of the normalized mean streamflow anomaly in the US stands at 0.1, with most deviations occurring below the curve. The streamflow anomaly is calculated as the difference between Budyko-predicted value and an actual $\bar{Q}/\bar{P}$ value. Catchments below the curve exhibit an average anomaly of −0.14, contrasting with an anomaly of 0.07 for those above the curve. Analysis of catchments in GB as shown in Fig. 2b, reveals an average absolute streamflow anomaly of 0.08. Notably, most catchments fall above the curve, with an average anomaly of 0.09, while those below the curve exhibit an anomaly of −0.06.

To further investigate the deviations from the Budyko curve, we analyze their relationships with alterations in water-energy balance as shown in Fig. 3a, b for the US and GB, respectively. The *z*-axis illustrates streamflow anomalies from the Budyko curve, while the *x*- and *y*-axes represent the causal relationships between streamflow-precipitation and streamflow-aridity, respectively, reflecting the water-energy balance of the catchments. The causal strength is measured based on the MCI test statistic value, and allows the ranking of causal links in a meaningful way[66,72]. MCI test statistic value ranges from −1 to 1, with +1 denoting the strongest positive link, while −1 represents the strongest link with a negative impact. The observations are then projected over the *x*- and *y*-axes in panels (c) and (e) of Fig. 3 for the US and panels (d) and (f) for GB.

In the US, the projection over *y*-axis as shown in Fig. 3e demonstrates a significant correlation (Spearman $\rho = -0.51$) between deviation from the Budyko curve (i.e., streamflow anomaly) and changes in the causal strength. This indicates that AR-Q predominantly influences deviations from the Budyko curve in the US. In GB, projection over *x*-axis in Fig. 3d highlights a significant correlation (Spearman $\rho = -0.54$) between streamflow anomaly and P-Q. This suggests that changes in P-Q mainly govern deviations from the Budyko curve in GB.

To ensure that our findings are not unduly influenced by the wide range of aridity indices present in the US catchments, we conducted an additional analysis focusing solely on humid catchments in the US (PET/P < 1). The overall pattern of correlation between streamflow anomalies and causal relationships remains consistent when considering only humid US catchments (See Supplementary Fig. 1). Specifically, the correlation between streamflow anomaly and AR-Q causal strength decreased slightly from Spearman ρ of −0.51 for all US catchments to Spearman ρ of −0.46 for humid US catchments. Both correlations are statistically significant, indicating that our conclusions are robust even when focusing solely on humid catchments.

The percentage of cropland and snow fraction may explain certain deviations from the Budyko curve

We further investigate the impact of changes in CL% and snow fraction (SF) on the causal dynamics between P-Q and AR-Q. This exploration can partly explain deviations from the Budyko curve. Similar to Fig. 3, the long-term observations of catchments within the Budyko framework are projected over *x*- and *y*-axes in Fig. 4, stratified by the snow fraction impact (i.e., SF-Q) in panels (a) and (b) for the US and GB, respectively. Panels (c) and (d) display the influence of the long-term CL% for the US and GB, respectively.

Examining Fig. 4a, c reveals that both snow fraction and CL% play crucial roles in influencing deviations from the Budyko curve by altering AR-Q causal relationship. The snow fraction impact strengthens as points move below the Budyko curve, demonstrating a significant association with the AR-Q relationship (Spearman $\rho = -0.48$) for catchments below the curve. The heightened influence of snow fraction is associated with the AR-Q causal relationship, contributing to increased deviations from the Budyko curve. Regarding CL%, catchments above the Budyko curve generally exhibit higher CL%. The CL% is significantly associated with the AR-Q causal relationship (Spearman $\rho = -0.53$). The elevated role of aridity, associated with higher CL%, amplifies deviations from the Budyko curve.

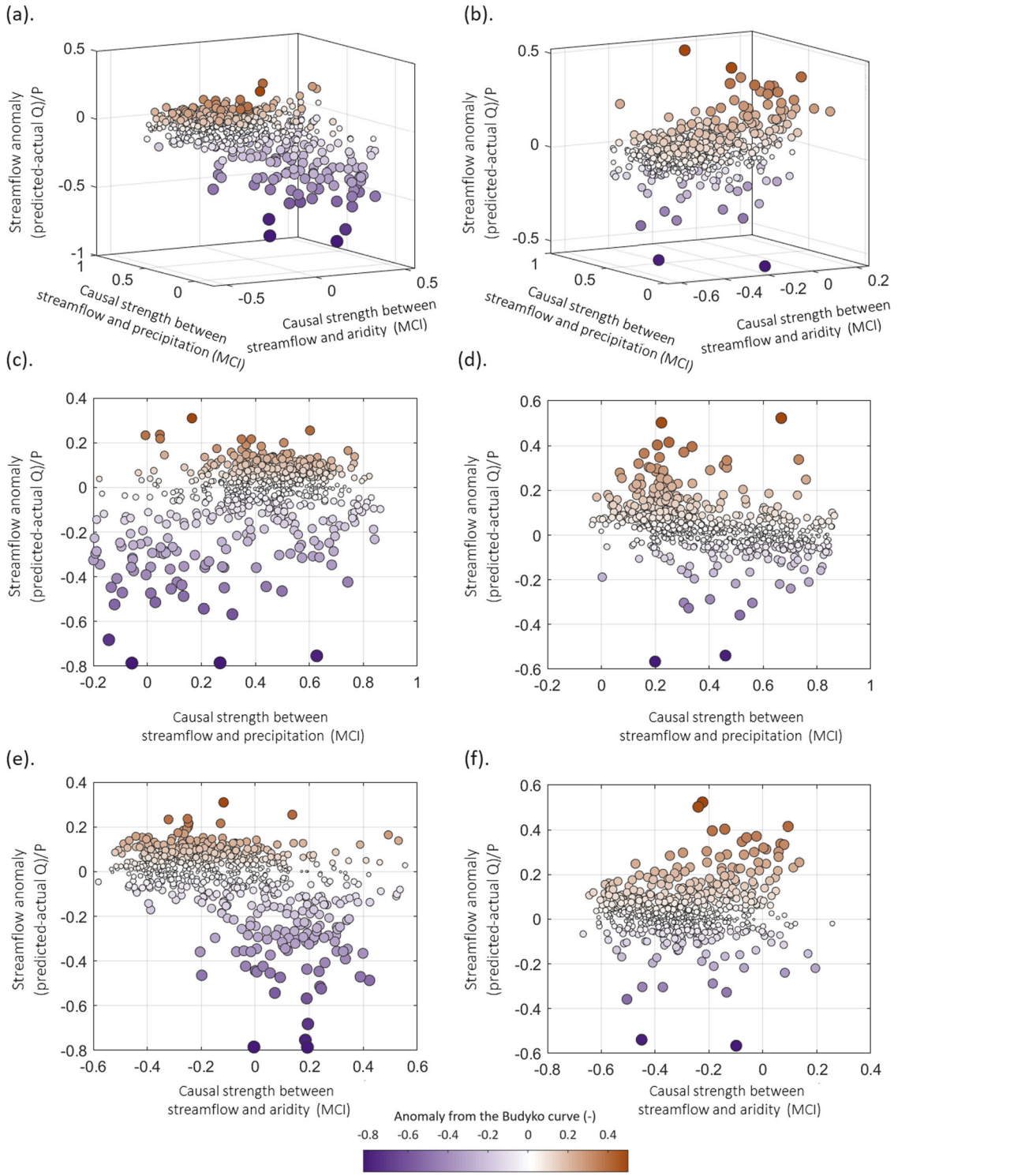

Fig. 3 | Analysis of long-term observed anomalies from the Budyko curve. The long-term observed anomalies from the Budyko curve are analyzed through a water-energy balance for the US and GB, as depicted in (**a**, **b**), respectively. The *z*-axis depicts anomalies from the Budyko curve, while the *x*- and *y*-axes display the causal strengths between streamflow-precipitation and streamflow-aridity, respectively, reflecting the water-energy balance of the catchments. The projections of the observations over the *x*- and *y*-axes are shown in (**c**) and (**e**) for the US and panels (**d**) and (**f**) for GB.

In contrast, as there is barely any snow in the GB's catchments, the role of snow fraction is negligible. Instead, CL% plays a pivotal role in altering the P-Q relationship, revealing a strong association between CL% and the P-Q relationship (Spearman $\rho = -0.89$). Higher CL% weakens the strength of the P-Q causal relationship, linked to more pronounced deviations from the Budyko curve (See Supplementary Fig. 3 for a better understanding of the varied effect of agriculture on the causal relationships). The geographical distribution of the individual CAMELS catchments and the corresponding percentages of crop area are shown in Supplementary Figs. 4 and 5. It is worth noting that while other researchers may propose (slightly) different equations to describe the Budyko curve, the conclusions regarding the impact of agriculture remain consistent no matter which equation is used (See Supplementary Fig. 6). The same consistency applies to the conclusion regarding snow fraction.

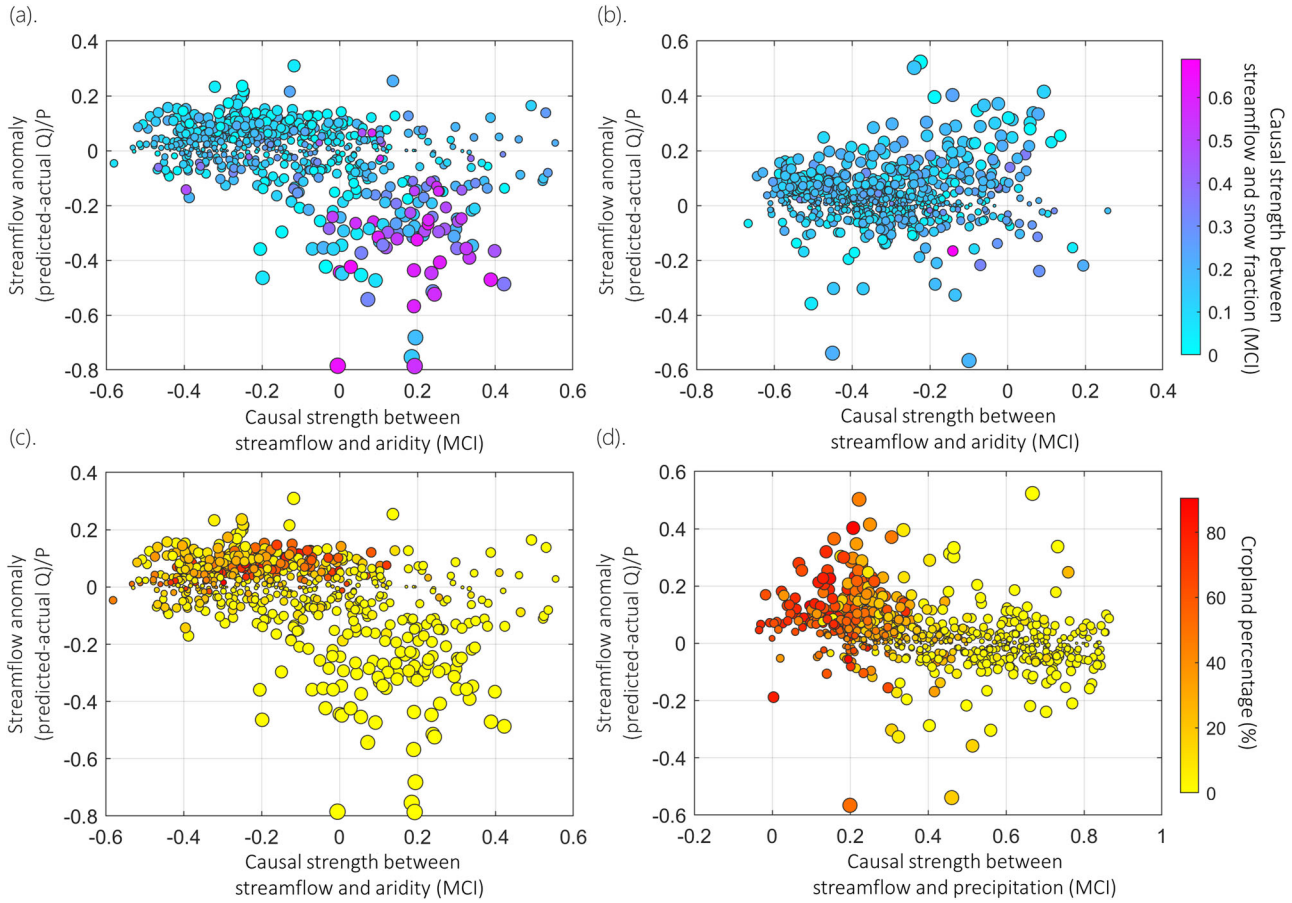

Fig. 4 | Impact of Snow fraction and cropland percentage on water-energy balance. The analysis of snow fraction (SF) and cropland percentage (CL%) and their associations with casual relationships between streamflow-aridity-precipitation. **a**, **b** present snow fraction analysis for the US and GB, respectively. **c**, **d** depict the analysis of CL% for the US and GB, respectively. The points are stratified by shades of blue and red colors across the first and second rows to distinguish between the impacts of SF and CL%. The *y*-axes represent the deviations from the Budyko curve (i.e., streamflow anomalies), while *x*-axes indicate the causal strength between aridity/precipitation and streamflow. Only significant patterns are presented here for brevity, and additional details can be found in Supplementary Figs. 2 and 3.

Causal relationships suggest that agriculture in the US and GB rely on different water sources

The preceding analysis implies different impacts of agriculture on the interplay among streamflow, precipitation, and aridity. In GB, causal analysis reveals a direct impact of agriculture on P-Q relationships, indicating that the weakening of P-Q causal relationship is associated with increases in CL% in a catchment. However, this is not observed in the US, where the impact of agriculture on the AR-Q relationship is more pronounced. As shown in Fig. 4 and Supplementary Fig. 2, the percentage of crops has a strong relationship with the causal strength between precipitation and streamflow in GB, indicating that precipitation is the primary source of agriculture in these areas. This is evidenced by a strong Spearman correlation coefficient of −0.89, with a 95% confidence interval spanning from −0.90 to −0.87. Conversely, in the US, Supplementary Fig. 3 reveals a weak correlation between CL% and the causal strength between precipitation and streamflow, as indicated by a Spearman correlation coefficient of 0.12 with a 95% confidence interval ranging from 0.05 to 0.2.

Hence, to better understand the sources of water for agriculture in the US, we partition streamflow into two components: direct flow (Qd; immediate runoff-fed component) and baseflow (Qb; groundwater-fed component[73,74]) utilizing a one-parameter low-pass filter[11,12,75–78] (See "method" section for details). We examine the relationship between the rate of change in the annual baseflow (i.e., groundwater-sustained river flows) and the CL% to understand the impact of CL% on the changes in the baseflow—Please consult Supplementary Figs. 7 and 8 for a detailed analysis of the connections between variations in baseflows, groundwater levels, and their relationship with CL% in selected US catchments.

Agricultural catchments in the US experience decreases in baseflow, suggesting groundwater is the main source of agricultural water

In Section "Causal relationships suggest that agriculture in the US and GB rely on different water sources", we identified distinct patterns between the US and GB catchments: in GB, changes in the P-Q relationship were significantly influenced by CL%, whereas in the US, the AR-Q relationship showed stronger associations with agricultural practices. To further investigate the underlying mechanisms driving these differences, Section "Agricultural catchments in the US experience decreases in baseflow, suggesting groundwater is the main source of agricultural water" focus on baseflow dynamics, hypothesizing that the contrasting behaviors of P-Q-AR relationships might stem from differences in water sources for agriculture. We calculate the linear regression trend of normalized annual baseflows (TNB) over the study period and examine its relationship with the percentage of crop cover in the agricultural catchments.

Figure 5 summarizes these findings, with the *y*-axis representing TNBs and the x-axis denoting CL%. Panels (a) and (b) display the results for the US and GB, respectively. The TNBs are determined through a simple linear regression trend, with dashed lines indicating the significance level (i.e., regression trend) at p-value = 0.05.

In the US, a strong correlation emerges between the rate of change in baseflow and crop cover, with a Spearman correlation coefficient of −0.45 and a 95% confidence interval spanning from −0.52 to −0.38. Notably, 42% of catchments in the US exhibit negative trends, with 7.1% being statistically significant. Conversely, in GB, the relationship between TNBs and crop cover appears to be relatively weak, indicated by a Spearman correlation

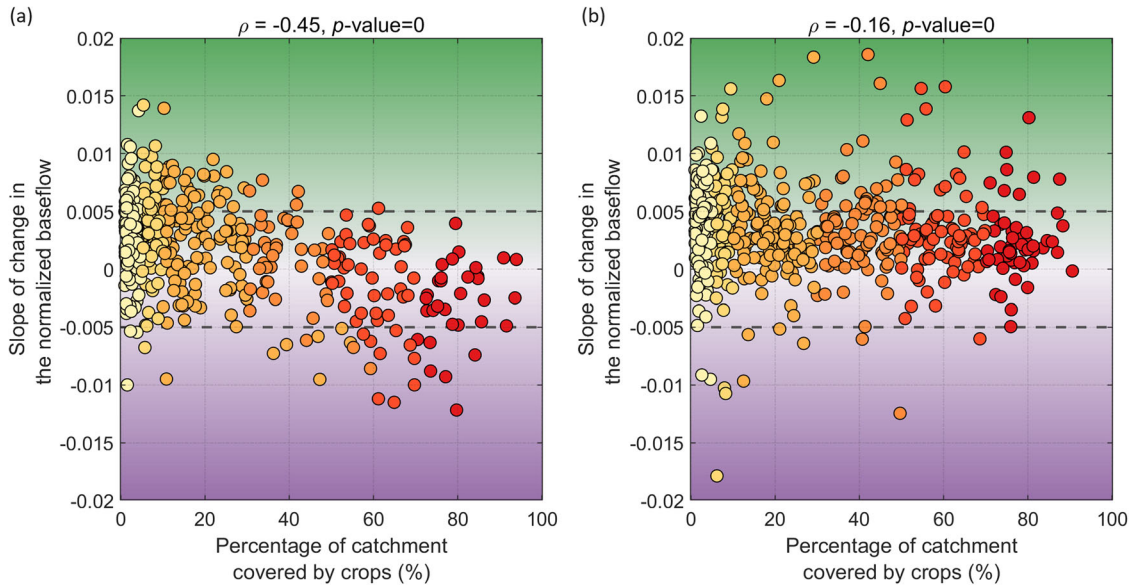

Fig. 5 | Trends in normalized baseflows in relation to cropland percentage. Analysis of change in the normalized baseflows for the catchments in the US and GB, which contain at least 1% of cropland as a percentage of the total basin area shown in (**a**, **b**), respectively. The dashed lines demonstrate the significance level (i.e., the threshold for regression trend) for p-value = 0.05. The significance threshold is defined to detect instances of significant negative trends in baseflows. The y-axis is the linear regression trend of the normalized baseflow, and the x-axis is the percentage of catchment covered by crops. In the US, the regression trend of the baseflow is highly correlated with CL% (Spearman $\rho = -0.45$), with 7.1% of catchments showing significantly negative trends. In GB, however, the linear regression trend in the baseflow is barely correlated with CL% (Spearman $\rho = -0.16$), with only 2.3% of catchments showing significantly negative trends. To account for the sensitivity of the results to the cropland percentage, we repeat the analysis for the catchments with a 5% cropland percentage—See Supplementary Fig. 11.

coefficient of −0.16, with a 95% confidence interval spanning from −0.26 to −0.06. A mere 13.2% of agricultural catchments in GB display negative trends in baseflow, with only 2.4% being statistically significant not attributable to agricultural practices. It is worth noting that we also conducted a trend analysis for precipitation, suggesting no significant decrease in annual precipitation at a significance level of 0.05 (p-value = 0.05) for the catchments over the studied period (See Supplementary Figs. 9 and 10).

Discussion

Improving our understanding of changes in streamflow and its attribution to human intervention and climate is important, as unravelling drivers of changes is vital for water resources management and planning. Previous work has focused on the Budyko framework to analyze the sensitivity of streamflow to changes in a few controlling variables. The Budyko framework is useful in explaining spatial differences in streamflow across natural catchments, but it is limited in explaining temporal changes in streamflow within catchments, particularly in the face of climate change and human activities. Additionally, its use for analyzing water availability sensitivity at finer temporal scales is debatable due to space-time asymmetry[22]. Consequently, the extent to which human interventions and climate control water availability remain uncertain, especially at finer temporal resolutions. This study addresses this gap by employing the PCMCI+ causal discovery algorithm (1) to explain how alterations in the water-energy balance can explain deviations from the Budyko curve and (2) to associate these alterations with climate and human intervention.

Our findings highlight that alterations in water-energy balance contribute to deviations from the Budyko curve, showcasing unique patterns in the US and GB. This pattern can first be attributed to the primary sources of water for agriculture and the distinct hydroclimatic conditions prevailing in each country. In the US, particularly in water-limited catchments, groundwater is a significant source of water for agriculture[28,37,79]. In these catchments, crop cover percentage (CL%) is significantly associated with the aridity-streamflow (AR-Q) relationship (Supplementary Fig. 3). The relationship between CL% and the AR-Q relationship indicates that higher crop cover in one catchment is associated with a stronger and negative relationship between aridity and streamflow. This is because groundwater pumping for irrigating more percentage of crop cover in one catchment can enhance evapotranspiration, reducing surface streamflow in catchments where water is primarily sourced from groundwater[31,80–82]. This aligns with previous literature, such as studies demonstrating the substantial impact of groundwater-fed irrigation in the US High Plains on evapotranspiration and alterations in water-energy balance[83]. For instance, it is demonstrated that groundwater-fed irrigation in the US High Plains, contributes more than half of the increase in evapotranspiration from the period of 1940–1975 to 1976–2010[79], leading to alteration in the water-energy balance. Our findings related to the role of groundwater-fed agriculture in deviations from the Budyko water-energy balance through changing AR-Q relationship are also confirmed in other research, indicating that the theoretical relationship between dryness and evaporative index is more likely impacted by groundwater losses or gains[24,25,84].

It is also revealed that groundwater losses affect streamflow and evapotranspiration across the US[83]. The role of irrigated cropland in changing water-energy balance is highlighted through changing evapotranspiration[85,86]. It is demonstrated that energy fluxes and evapotranspiration were significantly affected by crop development[84,85,87], confirming the effect of cropland in altering energy balance. However, the P-Q relationship in the US is not significantly associated with CL% in agricultural catchments (Fig. 4), possibly due to the predominant reliance on groundwater rather than direct precipitation for agricultural needs. This aligns with other research in the literature, indicating that increases in streamflow intermittency may be primarily observed in regions with ongoing storage losses due to pumping-induced groundwater in the US[43,88,89].

Conversely, in GB, where catchments are energy-limited, and precipitation is the main source of water for agriculture, alterations in water-energy balance primarily stem from changes in the strength of causal relationships between streamflow and precipitation (P-Q). Unlike the US, where agriculture is linked to AR-Q relationships, in GB, the CL% shows a strong association with the P-Q relationship (Fig. 4 and Supplementary Fig. 3). As CL% increases, the P-Q relationship decreases, indicating that higher crop cover is linked to reduced streamflow. This can be attributed to increased evapotranspiration and water uptake by plants, which is more pronounced in catchments where agriculture depends heavily on

precipitation[84,90]. The lack of correlation between CL% and the AR-Q relationship in GB can be attributed to the relatively humid climate, where aridity is less of a limiting factor for streamflow than the US[91,92]. Studies in GB show that high levels of water use by crops could result in less repartition of precipitation in favor of evapotranspiration rather than runoff[26,91,92].

Besides agriculture, snow fraction also plays a role in perturbing water-energy balance in US catchments, influencing the AR-Q relationship. As the influence of snow fraction intensifies, deviations from the Budyko curve become more prominent, with points moving below the curve (Fig. 4). This corresponds with existing findings that highlight the significance of snow fraction in controlling streamflow and its association with deviations from the Budyko curve in the US[14]. Studies reveal that a reduction in albedo from snow loss and the resulting increase in solar radiation absorption are the primary causes of increased evapotranspiration, which in turn causes a decrease in streamflow in snowy catchments[6,7,45]. Research on streamflow elasticity in snowy catchments consistently demonstrates low elasticity values, indicating the buffering effect of snow on streamflow response to precipitation and solar energy absorption[41,93]. This confirms our findings regarding the low strength of causal relationships between streamflow and precipitation in snowy catchments (See Supplementary Fig. 12e). The results of this study are based on the CAMELS datasets. However, potential evapotranspiration can be calculated using various methods, which may affect the study's outcomes[57,94]. Further research is required to assess the impact of different PET calculation methods on the results.

In summary, this study revealed the role of agriculture, specifically CL %, and snow fraction on altering water-energy balances in both the US and GB, as supported by findings from others in the literature. The distinct associations with AR-Q and P-Q relationships underscore the unique agricultural practices and hydroclimatic conditions prevalent in each region. While our analysis primarily focused on the deviations from the Budyko curve due to alterations in water-energy balance caused by agriculture and snow fraction, there are additional influential factors, such as climatic variables (e.g., climate variability and change), anthropogenic activities (e.g., drainage and groundwater extraction for domestic and industrial use), and catchment characteristics, that can also exert influence on the regional and global hydrological patterns. For instance, in the Southeast region of GB, where the majority of agricultural activities take place, there are instances of low runoff coefficient values during rainfall-runoff events in chalk catchments characterized by high permeability[95]. In these areas, lateral subsurface flow in chalk catchments is a factor to consider. However, given that the water involved would likely travel quickly through the saturated zone and subsequently would contribute to flow over the course of months[96,97], its presence or absence does not significantly impact the arguments presented in this paper.

In attributing the water-energy balance to CL% as a proxy for agriculture, there is an opportunity for further research into the interplay of human and natural hydrological dynamics. For instance, a more comprehensive investigation of precipitation-streamflow in GB can provide insights into the relationship between changes in the hydrologic cycle, CL%, and the implementation of field drainage in the 1970s and early 1980s[98]. This, in turn, can unveil how agricultural practices aimed at reducing waterlogged conditions have impacted crop yield, transpiration, and water storage capacity within the upper soil profile, leading to runoff changes[99,100]. These multifaceted interactions warrant continued exploration and consideration in our ongoing efforts to address water-related challenges and secure a more sustainable future.

Data and method

Data

The analyzed watersheds come from two distinct datasets, one covering the US and the other focusing on GB. In the US dataset, catchments are chosen from the CAMELS dataset[101], encompassing discharge, meteorological data, and various attributes for 671 catchments spanning the contiguous US. These catchments are distributed across the contiguous US and vary in size, ranging from 4 to 25,817 km². The dataset includes daily time series data from 1980 to 2015, encompassing precipitation, temperature, potential evaporation, and streamflow. Potential evapotranspiration is estimated by N15 meteorological forcing data—an extension of the Newman et al.[102] dataset—using Priestley–Taylor formulation calibrated for each catchment. The streamflow data can be directly extracted from the HCDN-2009 network[103]. This data is accessible via the USGS website (https://waterdata.usgs.gov/nwis, last accessed on 12 August 2023). Additionally, percentage cropland extent percentage (CL%), a designated area of land specifically utilized for cultivation, planting, and harvesting of crops, was derived from the global cropland map[104]. The groundwater-level data are available from the US Geological Survey (https://waterdata.usgs.gov/nwis/inventory).

For GB, the catchment data is sourced from the CAMELS-GB dataset[105], which offers hydrometeorological and attribute information for 671 catchments across GB. These catchments exhibit diverse sizes, ranging from 1.6 to 9930 km², and the dataset provides daily time series data for various variables, including temperature, precipitation, potential evapotranspiration, and streamflow, covering the period from 1970 to 2015. In CAMELS-GB, daily potential evapotranspiration time series were derived from the Climate Hydrology and Ecology research Support System Potential Evapotranspiration dataset (CHESS-PE[106]) using Penman-Monteith equation. The cropland percentage values can be directly obtained from CAMELS-GB dataset. Detailed explanations of the CAMELS datasets are available in Coxon et al.[105] and Addor et al.[101].

Primary climatic streamflow drivers

To apply the PCMCI+ algorithm and gain a deeper understanding of the factors affecting water balance, we must identify the primary drivers of streamflow variations. In this context, we focus on three crucial factors that impact streamflow (Q): precipitation (P), aridity (AR), and snow fraction (SF) time series. The selection of these variables is based on their well-documented importance as climatic factors influencing streamflow, supported by previous research[20,107–111]. However, to ensure that aridity was the best choice, we conducted a comparative analysis using potential evapotranspiration (PET) to evaluate its effectiveness relative to aridity in explaining streamflow changes (See Supplementary Figs. 13 and 14). The results indicated that the aridity index can better explain streamflow variations than PET, confirming the suitability of aridity as a primary driver in our study.

Although the Budyko framework traditionally represents streamflow anomalies as deviations in Q/P, we chose to focus our causal analysis on Q alone. This decision is because Q, as the direct hydrological output of the catchment, is more sensitive to and reflective of the climatic drivers we aim to investigate. Additionally, the aridity index (AR or PET/P) already incorporates P in its denominator, and including Q/P as the dependent variable alongside AR would introduce redundancy and complicate the interpretation of the causal relationships. Precipitation (P) is a dynamic input that directly influences Q, and analyzing Q allows for a clearer understanding of the causal mechanisms. By contrast, Q/P normalizes the streamflow by precipitation, which can obscure the direct influence of these drivers. Thus, focusing on Q provides a more interpretable approach for uncovering the causal relationships driving streamflow variability, consistent with the objectives of this study and supported by previous research[14,20,107,112–114].

Precipitation and aridity data are directly sourced from the Camels datasets. To determine the portion of precipitation that falls as snow (Snow Fraction; SF), a simple temperature-based threshold was utilized. If the average temperature for a given day was below 1° Celsius, all precipitation was classified as snowfall[14]. Conversely, when temperatures exceeded 1° Celsius, the precipitation was categorized as rainfall. An alternative threshold of 0° Celsius[70] is also explored, with consistent results, regardless of the chosen method for estimating snowfall. To run the PCMCI+ algorithm, the daily time series are then aggregated into seasonal time series.

To run the PCMCI+ algorithm, the daily time series are aggregated into seasonal time series. This decision is rooted in the recognition that seasonal data captures key hydrological interactions that occur over shorter

time scales, which are often missed in Budyko-based studies that rely on long-term temporal averages[21]. By analyzing the data at a seasonal scale, we account for the in-phase and out-of-phase dynamics of water (precipitation) and energy inputs (aridity and snowmelt), which are critical in shaping streamflow variability[115,116]. These dynamics are masked at annual scales but become evident in seasonal analyses, providing a clearer understanding of the causal relationships between streamflow and its climatic drivers. Furthermore, while finer temporal scales (e.g., daily or monthly) may offer additional insights, they introduce complexity, such as the need for time lag adjustments in processes, making the seasonal scale the most appropriate for this study.

Budyko framework

The research utilizes the Budyko framework, a widely accepted method for examining the interactions between streamflow elements, climate, and catchment features in the long-term water balance[10,11,15]. This framework formalizes the partitioning of precipitation (P) into evapotranspiration (ET) and runoff (Q) as a function of aridity through the Budyko curve. It serves as a valuable tool for assessing the primary controlling factors of water balance components. By examining the deviations of catchments with specific characteristics from the Budyko curve, we can assess how and to what extent these attributes influence the water balance components beyond the aridity index (ϕ)[14,21].

The Budyko curve used for normalizing long-term water balances of catchments is represented by the following equation[10]:

$$\frac{1-\bar{Q}/\bar{P}}{\bar{P}} = \sqrt{\frac{\bar{E}_p}{\bar{P}}\tanh\left(\frac{\bar{P}}{\bar{E}_p}\right)\left(1-\exp\left(-\frac{\bar{E}_p}{\bar{P}}\right)\right)} \quad (1)$$

where $\bar{Q}$, $\bar{P}$, and $\bar{E}_p$ denote the long-term mean values for streamflow, precipitation, and potential evaporation.

We employed the non-parametric Budyko curve due to its robustness and ability to capture complex hydrological responses across heterogeneous regions without imposing arbitrary parameters. This approach aligns with our exploratory analysis goals, allowing for consistent comparisons between catchments in the US and UK, regardless of local calibration. The non-parametric curve avoids the limitations of parametric formulations, such as potential inaccuracies and the speculative nature of parameter values, while maintaining the generality and facilitating a meaningful exploration of hydrological differences influenced by agricultural practices.

Causal discovery algorithm

Using the Budyko hypothesis, we examine the spatial impact of agriculture on the water cycle across catchments. This approach, however, does not account for the influence of precipitation changes on streamflow components, and spatial differences in water balance can be attributed to different factors. Additionally, most studies of statistical attribution of changes in streamflow typically employ qualitative reasoning, sensitivity-based analysis and/or correlation-based techniques to show consistency between changes detected and typically a single driver with little effort to systematically quantify the assumed cause–effect relationship[14,22,117]. To enhance our understanding, a fundamental question is how these variables causally interact with each other. This requires the identification of directional dependencies based on conditional independence relations in data series. Here, having the observed time series, we can exploit the temporal information of the observations for identifying causal graph[118].

Formally, we consider a variable $X^i_{t-\tau}$ as part of a multivariate stochastic process X, where i is the variable index (e.g., $i\epsilon\{Q, P, AR, SF\}$, and t is the time index. A variable that causally affects another is termed as the driver, while the affected variable is the target. Unlike bivariate correlation analysis, causal discovery algorithms can exclude dependencies between two variables that arise from common drivers $X^i_{t-\tau_1} \leftarrow X^S_{t-\tau_2} \rightarrow X^j_t$ or indirect paths ($X^i_{t-\tau_1} \rightarrow X^S_{t-\tau_2} \rightarrow X^j_t$), where S is a conditioning set and τ is a time lag. For instance, when estimating the effect of P on Q and SF on Q using bivariate measures (e.g., using bivariate correlation or sensitivity analysis), one might obtain misleading results to unaccounted drivers like surface air temperature, as the common driver and mediator (indirect path). A causal discovery graph algorithm can exclude such dependencies using conditional independence tests, denoted as $CI(\{X^i_{t-\tau}, X^j_{t-\tau}|S\})$, where S is a conditioning set.

Two key methods for assessing directional dependencies are Granger causality and transfer entropy. Both methods can be used to test for conditional independence. However, in their original bivariate forms, they do not account for third variables, and extending transfer entropy to multivariate cases is challenging due to the curse of dimensionality[119], and low link detection power for limited sample size, as is the case in our application[66].

To address these issues and understand how factors like snow fraction, aridity, and precipitation[14,20,70,71] impact streamflow across different catchments in the US and GB, we utilized Peter–Clark Momentary Conditional Independence Plus Algorithm (PCMCI+)[64,66,120,121]. PCMCI+ addresses the challenges of identifying contemporaneous and time-lagged causal links in autocorrelated high-dimensional time series[69]. It employs a two-step approach that combines a variant of the PC algorithm[122] and the MCI measure[66] to assess the causal structure of a multivariate dataset or process X by estimating its time series graph.

Here, we make the following assumptions for the time series: contemporaneous causal effects, causal stationarity, faithfulness, and causal sufficiency (See Runge[118]). The faithfulness and causal Markov assumptions relate the underlying physical causal mechanisms to the statistical relations observed in the data. Causal sufficiency implies that all the variables include all common causes, following the principle[123]. These assumptions relate conditional independence to *d-separation* in the graph under this distribution: $Xd-\text{sep}Y|Z \Longleftrightarrow X \perp Y|Z$, where the forward and backward effects are associated with the causal Markov and causal faithfulness assumptions, respectively. Pearl[63] states that two nodes are *d-separated* given Z if and only if Z blocks all pathways between them. The situation in which X influences Y by two opposing and mutually exclusive effects is ruled out by the causal faithfulness assumption. According to the causal sufficiency assumption, any common cause of two or more variables $X^i \in X$ is included in X. Causal stationarity refers to the existence of links over time.

The causal sufficiency assumption, which suggests that all common drivers are included in the analysis, is inherently challenging to test and conceptualize, particularly in catchment hydrology[124,125]. This complexity arises due to data constraints and the intricate nature of environmental systems[126]. While factors like topography influence various processes, it is often impractical to account for every impactful variable. Recognizing these limitations allows us to interpret our findings within the context of available data, while understanding that unobserved variables could influence the results[125].

PCMCI offers a robust approach for handling such challenges compared to many other methods[126]. It uses momentary conditional independencies to detect causal relationships and can partially account for unobserved confounders by observing changes in dependence structures. While no method is perfect, PCMCI's ability to provide causal inference by incorporating temporal dynamics and refining causal graphs provides valuable insights, making it particularly effective in dealing with the complexities of real-world data where not all influencing factors can be directly measured[66,125,126].

The PC algorithm starts with a directed acyclic graph (DAG) to identify causal links between variables. The graphical representation in Fig. 6a–c outlines the causal structure of the system, where variables x_k ($k = 1, \ldots, 4$) are represented by nodes and causal interactions are indicated by directed edges. The PCMCI+ technique was used to construct the DAG[66,69]. There are two phases to the algorithm. Initially, the PC_1, a Markov set discovery algorithm based on the Peter–Clark PC-stable algorithm[121], starts with a fully connected graph (See Fig. 6a). This algorithm assumes that causal links are stationary.

PC algorithm then examines for the removal of links between variables iteratively by conditioning sets of increasing cardinalities (See Fig. 6b). The

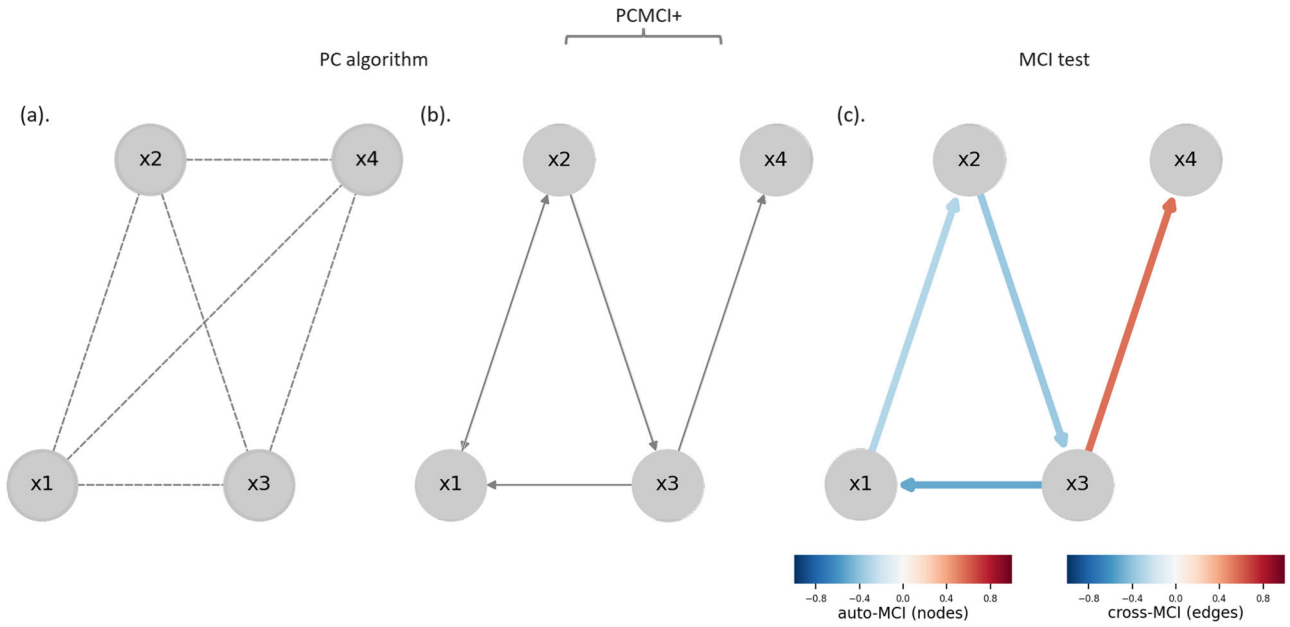

Fig. 6 | Overview of the PCMCI+ causal discovery graph algorithm. Overview of the PCMCI+ causal discovery graph algorithm. The variables x_k ($k = 1, \ldots, 4$) are depicted by nodes and causal interactions are indicated by directed edges. It includes two main steps (PC algorithm) and MCI tests. PC_1 starts with a fully connected graph as shown in (**a**). It then tests for the elimination of links between variables iteratively by conditioning sets of increasing cardinalities as shown in (**b**). MCI tests use the estimated conditions found in step one to infer a causal link—See (**c**). The node colors indicate the level of auto-dependency (auto-MCI) of each component and link colors indicate the interdependency strength (cross-MCI) between variables.

conditional independence tests, $CI(\{X^i_{t-\tau}, X^j_t|S\})$, are the fundamental components of PC_1. They are used to evaluate $\{X^i_{t-\tau}, X^j_t|S\}$ given a conditioning set S. It considers expanding cardinality conditioning sets while iteratively testing for conditional independence under a growing number of conditions. In order to estimate $CI(\{X^i_{t-\tau}, X^j_t|S\})$ efficiently, it is imperative that the conditioning set S be as small as possible, including only relevant conditions. This enables us to separate out the unique impact of $X^i_{t-\tau}$ on X^j_t. To further eliminate false links and enhance detection power, the method iterates over contemporaneous conditions using MCI tests for all ordered pairs.

Here, we employ the partial correlation (ParCorr) conditional independence test to determine independence. Partial correlations and the t test serve as the foundation for the ParCorr conditional independence test. Partial correlations and the t test serve as the foundation for the ParCorr conditional independence test. With the independence test's significance threshold set at 0.05, the PC algorithm can only converge to a small number of relevant conditions.

MCI tests. Using the estimated conditions found in step one, the MCI test infers a causal relationship in the second step—See Fig. 6c. MCI is indeed the causal discovery step that assigns a p-value and strength to each possible link. While the primary goal of the PCMCI+ algorithm is to detect the causal graph, MCI partial correlation values can be used to represent link strengths of causality[67], with the significance level set to 0.05 in the t test and is given by:

$$\mathrm{MCI}: X^i_{t-\tau} \perp X^j_t \left| \hat{\wp}(X^j_t) \{X^i_{t-\tau}\}, \hat{\wp}(X^i_{t-\tau}) \right. \tag{2}$$

where $\hat{\wp}(X^j_t)$ and $\hat{\wp}(X^i_{t-\tau})$ represent the parents of X^j_t and $X^i_{t-\tau}$ identified in the previous PC step, respectively; '\' means precluding $X^i_{t-\tau}$ from $\hat{\wp}(X^j_t)$.

In case of ParCorr, the strength, ranges from −1 to 1, is represented by the partial correlation value. In practice, ParCorr can also effectively detect non-linear relationships. When the linear component is particularly prominent compared to the non-linear aspects, ParCorr might outperform non-linear independence tests in terms of detection accuracy[66]. The Python software for estimating the causal network can be obtained from https://tocsy.pik-potsdam.de/tigramite.php.

To further validate the PCMCI+ algorithm prior to its application to real-world data, we tested it using an artificial dataset incorporates 4-dimensional (4D) stochastic linear vector autoregressive model with only one lag:

$$x_{1,t+1} = -0.5x_{3,t} + \xi_{1,t+1} \tag{3}$$

$$x_{2,t+1} = -0.3x_{1,t} + \xi_{2,t+1} \tag{4}$$

$$x_{3,t+1} = 0.5 - 0.4x_{2,t} + \xi_{3,t+1} \tag{5}$$

$$x_{4,t+1} = 0.2 + 0.7x_{3,t} + \xi_{4,t+1} \tag{6}$$

where the four time series x_k ($k = 1, \ldots, 4$) conceptually represent the four variables (SF, AR, P, Q), and the term ξ_k represents dynamical normal random noises in these four variables ($\xi_k \sim N(0, 1)$). By construction, we have one cycle, i.e., $x_1 \to x_2 \to x_3 \to x_1$ and x_3 drives x_4 (i.e., $x_3 \to x_4$).

Note that this test model is not designed to accurately represent observed processes; it is solely meant to evaluate the procedure. We generated artificial time series, each having a length equal to the studied time series. Here, we conducted a comparison between lagged correlation analysis and PCMCI+ on four generated time series, with the results presented in Fig. 7. Panel (a) depicts all potential connections among the four variables. Panel (b) shows the correlation coefficient matrix. Panels (c) and (d) display the PCMCI+ analysis outcomes, where (c) illustrates the causal graph and (d) presents the maximum path coefficients (MCI values). Only significant causal links with a p-value of 0.05 are highlighted in shades of blue and red. It is evident that the correlation analysis often fails to reveal true connections, instead highlighting a spurious relationship between x_1 and x_4. In contrast, PCMCI+ accurately uncovers the true causal relationships among variables. These false correlations can complicate the analysis, leading to incorrect conclusions and misleading hypotheses.

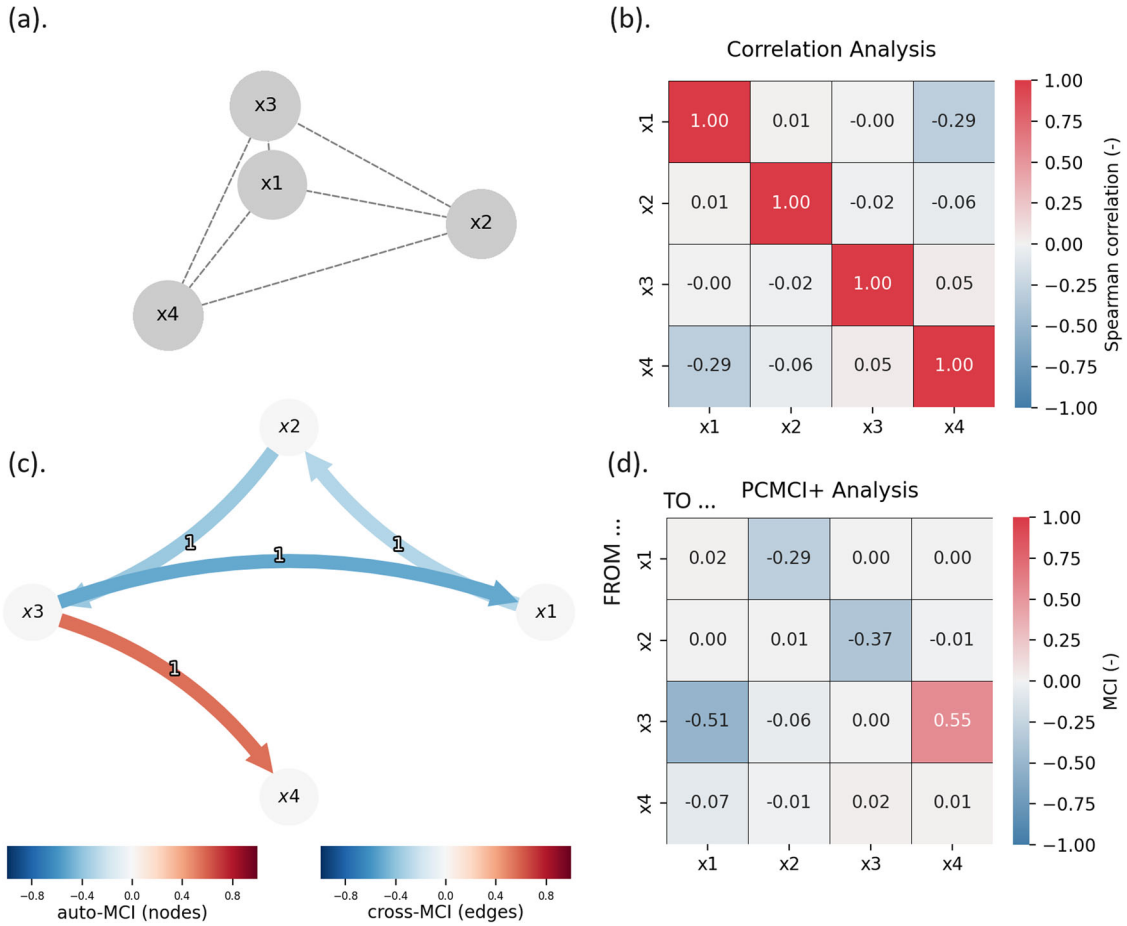

Fig. 7 | Comparison of PCMCI+ performance with correlation analysis. Overview of PCMCI+ performance compared to correlation analysis. Artificial datasets are generated with a prescribed interaction structure (Eqs. 3–6). **a** shows all possible links between the four variables. Here for the four generated time series, we compared the results of lagged correlation analysis and PCMCI+. **b** presents the matrix of correlation coefficients. **c**, **d** display the results of PCMCI+ analysis, with (**c**) showing the causal graph and (**d**) illustrating the maximum path coefficients (MCI values). Only causal links at a significance level of p-value = 0.05 are shown in shades of blue and red.

Decomposition of streamflow

To further explore the analysis of water sources for agriculture, we utilized a one-parameter low-pass filter method developed by Lyne and Hollick[75], commonly used in the literature[77,78,127] to effectively decompose streamflow into its constituent components, namely baseflow and direct flow. This method relies on temporal filtering principles, wherein the streamflow hydrograph undergoes convolution with a smoothing function defined by a filter parameter, often referred to as the recession constant (α). We applied the recursive filter iteratively three times (forward-back-forward) to filter off flood peaks from the original streamflow time series, configuring the filter parameter (set as 0.925; a widely accepted value in hydrological studies[11,75,78,127]). The resulting separation let us to discern the slow, groundwater-derived baseflow from the rapid, rainfall-induced direct flow. To account for the inherent uncertainty of streamflow partitioning[12], we repeated our analysis using the Lyne Holick one-pass configuration, which yielded quite similar results.

Reporting summary

Further information on research design is available in the Nature Portfolio Reporting Summary linked to this article.

Data availability

Daily hydro-meteorological timeseries and landscape attributes for 671 catchments across Great Britain (CAMELS-GB) are available from Environmental Information Data Centre available at https://catalogue.ceh.ac.uk/documents/8344e4f3-d2ea-44f5-8afa-86d2987543a9. The daily hydrometeorological time series along with the catchment attributes for the United States (CAMELS) are available from Geoscience Data Exchange Centre of National Science Foundation at https://gdex.ucar.edu/dataset/camels.html. The source data used to generate the figures in this manuscript are available at Zenodo: https://doi.org/10.5281/zenodo.13974112.

Code availability

The code used in this study to estimate the causal network is accessible through the Potsdam Institute for Climate Impact Research (PIK) at the following URL: https://github.com/jakobrunge/tigramite. Access to the code is unrestricted, allowing for replication and further development of the methods presented in this paper.

Received: 1 May 2024; Accepted: 8 November 2024;
Published online: 22 November 2024

References

1. Renner, M., Seppelt, R. & Bernhofer, C. Evaluation of water-energy balance frameworks to predict the sensitivity of streamflow to climate change. *Hydrol. Earth Syst. Sci.* **16**, 1419–1433 (2012).
2. Daly, E., Calabrese, S., Yin, J. & Porporato, A. Hydrological spaces of long-term catchment water balance. *Water Resour. Res.* **55**, 10747–10764 (2019).

3. Yang, H., Yang, D., Lei, Z. & Sun, F. New analytical derivation of the mean annual water-energy balance equation. *Water Resour. Res.* **44**, 3 (2008).
4. Chapin, F. S., Matson, P. A. & Vitousek, P. M. Water and energy balance. In *Principles of Terrestrial Ecosystem Ecology* (eds Chapin, F. S., Matson, P. A. & Vitousek, P. M.) 93–122 (Springer, New York, NY, 2011).
5. Padrón, R. S., Gudmundsson, L., Greve, P. & Seneviratne, S. I. Large-scale controls of the surface water balance over land: insights from a systematic review and meta-analysis. *Water Resour. Res.* **53**, 9659–9678 (2017).
6. Milly, P. C. D. & Dunne, K. A. Colorado river flow dwindles as warming-driven loss of reflective snow energizes evaporation. *Science* **367**, 1252–1255 (2020).
7. Goulden, M. L. & Bales, R. C. Mountain runoff vulnerability to increased evapotranspiration with vegetation expansion. *Proc. Natl. Acad. Sci.* **111**, 14071–14075 (2014).
8. Gordon, B. L. et al. Why does snowmelt-driven streamflow response to warming vary? A data-driven review and predictive framework. *Environ. Res. Lett.* **17**, 053004 (2022).
9. Condon, L. E., Atchley, A. L. & Maxwell, R. M. Evapotranspiration depletes groundwater under warming over the contiguous United States. *Nat. Commun.* **11**, 873 (2020).
10. Budyko, M. I. *Climate and Life*, Vol 508 (Academic, 1974).
11. Gnann, S. J., Woods, R. A. & Howden, N. J. K. Is there a baseflow Budyko curve? *Water Resour. Res.* **55**, 2838–2855 (2019).
12. Meira Neto, A. A., Roy, T., de Oliveira, P. T. S. & Troch, P. A. An aridity index-based formulation of streamflow components. *Water Resour. Res.* **56**, e2020WR027123 (2020).
13. Liu, J. & You, Y. The roles of catchment characteristics in precipitation partitioning within the Budyko framework. *J. Geophys. Res.: Atmos.* **126**, e2021JD035168 (2021).
14. Berghuijs, W. R., Woods, R. A. & Hrachowitz, M. A precipitation shift from snow towards rain leads to a decrease in streamflow. *Nat. Clim. Change* **4**, 583–586 (2014).
15. Wang, D. & Hejazi, M. Quantifying the relative contribution of the climate and direct human impacts on mean annual streamflow in the contiguous United States. *Water Resour. Res.* **47**, 10 (2011).
16. Yao, L., Sankarasubramanian, A. & Wang, D. Climatic and landscape controls on long-term baseflow. *Water Resour. Res.* **57**, e2020WR029284 (2021).
17. Cheng, S. et al. An analytical baseflow coefficient curve for depicting the spatial variability of mean annual catchment baseflow. *Water Resour. Res.* **57**, e2020WR029529 (2021).
18. Wu, J. et al. Dynamics and attributions of baseflow in the semiarid loess plateau. *J. Geophys. Res.: Atmos.* **124**, 3684–3701 (2019).
19. Reaver, N. G. F., Kaplan, D. A., Klammler, H. & Jawitz, J. W. Theoretical and empirical evidence against the Budyko catchment trajectory conjecture. *Hydrol. Earth Syst. Sci.* **26**, 1507–1525 (2022).
20. Berghuijs, W. R., Larsen, J. R., van Emmerik, T. H. M. & Woods, R. A. A global assessment of runoff sensitivity to changes in precipitation, potential evaporation, and other factors. *Water Resour. Res.* **53**, 8475–8486 (2017).
21. Berghuijs, W. R., Gnann, S. J. & Woods, R. A. Unanswered questions on the Budyko framework. *Hydrol. Process.* **34**, 5699–5703 (2020).
22. Berghuijs, W. R. & Woods, R. A. Correspondence: space-time asymmetry undermines water yield assessment. *Nat. Commun.* **7**, 11603 (2016).
23. Tan, X. & Gan, T. Y. Contribution of human and climate change impacts to changes in streamflow of Canada. *Sci. Rep.* **5**, 17767 (2015).
24. Liu, Y., Wagener, T., Beck, H. E. & Hartmann, A. What is the hydrologically effective area of a catchment? *Environ. Res. Lett.* **15**, 104024 (2020).
25. Bouaziz, L. et al. Redressing the balance: quantifying net intercatchment groundwater flows. *Hydrol. Earth Syst. Sci.* **22**, 6415–6434 (2018).
26. Rameshwaran, P. et al. Use of abstraction and discharge data to improve the performance of a national-scale hydrological model. *Water Resour. Res.* **58**, e2021WR029787 (2022).
27. Condon, L. E. & Maxwell, R. M. Groundwater-fed irrigation impacts spatially distributed temporal scaling behavior of the natural system: a spatio-temporal framework for understanding water management impacts. *Environ. Res. Lett.* **9**, 034009 (2014).
28. Scanlon, B. R. et al. Groundwater depletion and sustainability of irrigation in the US high plains and central valley. *Proc. Natl. Acad. Sci.* **109**, 9320–9325 (2012).
29. Zhang, J. et al. Sustainable irrigation based on co-regulation of soil water supply and atmospheric evaporative demand. *Nat. Commun.* **12**, 5549 (2021).
30. Yuan, T. et al. Effects of different irrigation methods on regional climate in North China plain: a modeling study. *Agric. For. Meteorol.* **342**, 109728 (2023).
31. Owuor, S. O. et al. Groundwater recharge rates and surface runoff response to land use and land cover changes in semi-arid environments. *Ecol. Process.* **5**, 16 (2016).
32. Döll, P. et al. Impact of water withdrawals from groundwater and surface water on continental water storage variations. *J. Geodyn.* **59–60**, 143–156 (2012).
33. Wada, Y., Wisser, D. & Bierkens, M. F. P. Global modeling of withdrawal, allocation and consumptive use of surface water and groundwater resources. *Earth Syst. Dyn.* **5**, 15–40 (2014).
34. Hoff, H. et al. Greening the global water system. *J. Hydrol.* **384**, 177–186 (2010).
35. Grafton, R. Q. et al. The paradox of irrigation efficiency. *Science* **361**, 748–750 (2018).
36. Griggs, D. et al. An integrated framework for sustainable development goals. *Ecol. Soc.* **19**, 4 (2014).
37. Steward, D. R. et al. Tapping unsustainable groundwater stores for agricultural production in the high plains aquifer of Kansas, projections to 2110. *Proc. Natl. Acad. Sci.* **110**, E3477–E3486 (2013).
38. Haacker, E. M. K., Kendall, A. D. & Hyndman, D. W. Water level declines in the high plains aquifer: predevelopment to resource senescence. *Groundwater* **54**, 231–242 (2016).
39. Meira Neto, A. A., Niu, G.-Y., Roy, T., Tyler, S. & Troch, P. A. Interactions between snow cover and evaporation lead to higher sensitivity of streamflow to temperature. *Commun. Earth Environ.* **1**, 1–7 (2020).
40. Cowherd, M., Leung, L. R. & Girotto, M. Evolution of global snow drought characteristics from 1850 to 2100. *Environ. Res. Lett.* **18**, 064043 (2023).
41. Sankarasubramanian, A., Vogel, R. M. & Limbrunner, J. F. Climate elasticity of streamflow in the United States. *Water Resour. Res.* **37**, 1771–1781 (2001).
42. Zhang, Y., Viglione, A. & Blöschl, G. Temporal scaling of streamflow elasticity to precipitation: a global analysis. *Water Resour. Res.* **58**, e2021WR030601 (2022).
43. Wieder, W. R. et al. Pervasive alterations to snow-dominated ecosystem functions under climate change. *Proc. Natl. Acad. Sci.* **119**, e2202393119 (2022).
44. Kim, Y., Kimball, J. S., Du, J., Schaaf, C. L. B. & Kirchner, P. B. Quantifying the effects of freeze-thaw transitions and snowpack melt on land surface albedo and energy exchange over Alaska and Western Canada. *Environ. Res. Lett.* **13**, 075009 (2018).
45. Liu, Q. et al. Hydrological effects of the snow fraction and its ecohydrological explication within the Budyko framework. *J. Hydrol.* **610**, 127813 (2022).
46. McColl, K. A., Roderick, M. L., Berg, A. & Scheff, J. The terrestrial water cycle in a warming world. *Nat. Clim. Chang.* **12**, 604–606 (2022).

47. Allan, R. P. et al. Advances in understanding large-scale responses of the water cycle to climate change. *Ann. N. Y. Acad. Sci.* **1472**, 49–75 (2020).
48. Zaerpour, M., Papalexiou, S. M. & Nazemi, A. Informing stochastic streamflow generation by large-scale climate indices at single and multiple sites. *Adv. Water Resour.* **156**, 104037 (2021).
49. Kirby, J. M. et al. The impact of climate change on regional water balances in Bangladesh. *Clim. Change* **135**, 481–491 (2016).
50. Duan, S., Pallotta, G. & Bonfils, C. Higher-order internal modes of variability imprinted in year-to-year California streamflow changes. *Commun. Earth Environ.* **5**, 1–11 (2024).
51. Wada, Y. et al. Global depletion of groundwater resources. *Geophys. Res. Lett.* **37**, 20 (2010).
52. Kåresdotter, E., Destouni, G., Ghajarnia, N., Lammers, R. B. & Kalantari, Z. Distinguishing direct human-driven effects on the global terrestrial water cycle. *Earth's Future* **10**, e2022EF002848 (2022).
53. Zhang, D., Cong, Z., Ni, G., Yang, D. & Hu, S. Effects of snow ratio on annual runoff within the Budyko framework. *Hydrol. Earth Syst. Sci.* **19**, 1977–1992 (2015).
54. Jaramillo, F. & Destouni, G. Developing water change spectra and distinguishing change drivers worldwide. *Geophys. Res. Lett.* **41**, 8377–8386 (2014).
55. Levi, L., Jaramillo, F., Andričević, R. & Destouni, G. Hydroclimatic changes and drivers in the Sava River catchment and comparison with Swedish catchments. *Ambio* **44**, 624–634 (2015).
56. Sun, L., Cai, Y., Chen, A., Zamora, D. & Jaramillo, F. Water footprint and consumption of hydropower from basin-constrained water mass balance. *Adv. Water Resour.* **153**, 103947 (2021).
57. Jaramillo, F. et al. Dominant effect of increasing forest biomass on evapotranspiration: interpretations of movement in Budyko space. *Hydrol. Earth Syst. Sci.* **22**, 567–580 (2018).
58. Helman, D., Lensky, I. M., Yakir, D. & Osem, Y. Forests growing under dry conditions have higher hydrological resilience to drought than do more humid forests. *Glob. Change Biol.* **23**, 2801–2817 (2017).
59. van der Velde, Y. et al. Exploring hydroclimatic change disparity via the Budyko framework. *Hydrol. Process.* **28**, 4110–4118 (2014).
60. Krajewski, A., Sikorska-Senoner, A. E., Hejduk, L. & Banasik, K. An attempt to decompose the impact of land use and climate change on annual runoff in a small agricultural catchment. *Water Resour. Manage.* **35**, 881–896 (2021).
61. Xing, W., Wang, W., Shao, Q. & Yong, B. Identification of dominant interactions between climatic seasonality, catchment characteristics and agricultural activities on Budyko-type equation parameter estimation. *J. Hydrol.* **556**, 585–599 (2018).
62. Puy, A. et al. The delusive accuracy of global irrigation water withdrawal estimates. *Nat. Commun.* **13**, 3183 (2022).
63. Pearl, J. *Causality*. (Cambridge University Press, 2009).
64. Pearl, J. *Causality: Models, Reasoning, and Inference*. xvi, 384 (Cambridge University Press, New York, NY, US, 2000).
65. Runge, J. et al. Inferring causation from time series in earth system sciences. *Nat. Commun.* **10**, 2553 (2019).
66. Runge, J., Nowack, P., Kretschmer, M., Flaxman, S. & Sejdinovic, D. Detecting and quantifying causal associations in large nonlinear time series datasets. *Sci. Adv.* **5**, eaau4996 (2019).
67. Runge, J. et al. Identifying causal gateways and mediators in complex spatio-temporal systems. *Nat. Commun.* **6**, 8502 (2015).
68. Nowack, P., Runge, J., Eyring, V. & Haigh, J. D. Causal networks for climate model evaluation and constrained projections. *Nat. Commun.* **11**, 1415 (2020).
69. Runge, J. Discovering contemporaneous and lagged causal relations in autocorrelated nonlinear time series datasets. In *Proc. 36th Conference on Uncertainty in Artificial Intelligence (UAI)* (eds Peters, J. & Sontag, D.) vol. 124, 1388–1397 (PMLR, 2020).
70. Knoben, W. J. M., Woods, R. A. & Freer, J. E. A quantitative hydrological climate classification evaluated with independent streamflow data. *Water Resour. Res.* **54**, 5088–5109 (2018).
71. Stein, L., Clark, M. P., Knoben, W. J. M., Pianosi, F. & Woods, R. A. How do climate and catchment attributes influence flood generating processes? A Large-sample study for 671 catchments across the contiguous USA. *Water Resour. Res.* **57**, e2020WR028300 (2021).
72. Ombadi, M., Nguyen, P., Sorooshian, S. & Hsu, K. Evaluation of methods for causal discovery in hydrometeorological systems. *Water Resour. Res.* **56**, e2020WR027251 (2020).
73. Freeze, R. A. Role of subsurface flow in generating surface runoff: 1. Base flow contributions to channel flow. *Water Resour. Res.h* **8**, 609–623 (1972).
74. Eckhardt, K. How to construct recursive digital filters for baseflow separation. *Hydrol. Process.* **19**, 507–515 (2005).
75. Lyne, V. & Hollick, M. Stochastic time variable rainfall-runoff modelling. https://scholar.google.com/scholar_lookup?hl=en&publication_year=1979&pages=82-92&author=V.+D.+Lyne&author=M.+Hollick&title=Hydrology+and+water+resources+symposium (1979).
76. Sivapalan, M., Yaeger, M. A., Harman, C. J., Xu, X. & Troch, P. A. Functional model of water balance variability at the catchment scale: 1. Evidence of hydrologic similarity and space-time symmetry. *Water Resour. Res.* **47**, 2 (2011).
77. Ballarin, A. S. et al. The impact of an open water balance assumption on understanding the factors controlling the long-term streamflow components. *Water Resour. Res.* **58**, e2022WR032413 (2022).
78. Berghuijs, W. R. & Slater, L. J. Groundwater shapes North American river floods. *Environ. Res. Lett.* **18**, 034043 (2023).
79. Zeng, R., Yao, C., Cai, X. & Haacker, E. Temporal and spatial pattern change in evapotranspiration over the high plains: the impact of and guide on extensive groundwater-fed irrigation. *Water Resour. Res.* **59**, e2023WR035004 (2023).
80. Chagas, V. B. P., Chaffe, P. L. B. & Blöschl, G. Climate and land management accelerate the Brazilian water cycle. *Nat. Commun.* **13**, 5136 (2022).
81. Brown, A. E., Zhang, L., McMahon, T. A., Western, A. W. & Vertessy, R. A. A review of paired catchment studies for determining changes in water yield resulting from alterations in vegetation. *J. Hydrol.* **310**, 28–61 (2005).
82. Bruijnzeel, L. A. Hydrological functions of tropical forests: not seeing the soil for the trees? *Agric. Ecosyst. Environ.* **104**, 185–228 (2004).
83. Condon, L. E. & Maxwell, R. M. Simulating the sensitivity of evapotranspiration and streamflow to large-scale groundwater depletion. *Sci. Adv.* **5**, eaav4574 (2019).
84. Chen, H., Huo, Z., Zhang, L. & White, I. New perspective about application of extended Budyko formula in arid irrigation district with shallow groundwater. *J. Hydrol.* **582**, 124496 (2020).
85. Wang, X. et al. Energy fluxes and evapotranspiration over irrigated maize field in an arid area with shallow groundwater. *Agric. Water Manag.* **228**, 105922 (2020).
86. Wang, X., Huo, Z., Feng, S., Guo, P. & Guan, H. Estimating groundwater evapotranspiration from irrigated cropland incorporating root zone soil texture and moisture dynamics. *J. Hydrol.* **543**, 501–509 (2016).
87. Liu, Z., Chen, H., Huo, Z., Wang, F. & Shock, C. C. Analysis of the contribution of groundwater to evapotranspiration in an arid irrigation district with shallow water table. *Agric. Water Manag.* **171**, 131–141 (2016).
88. Zipper, S. C. et al. Cannabis and residential groundwater pumping impacts on streamflow and ecosystems in Northern California. *Environ. Res. Commun.* **1**, 125005 (2019).
89. Zimmer, M. A. & McGlynn, B. L. Bidirectional stream–groundwater flow in response to ephemeral and intermittent streamflow and groundwater seasonality. *Hydrol. Process.* **31**, 3871–3880 (2017).

90. Cheng, L., Xu, Z., Wang, D. & Cai, X. Assessing interannual variability of evapotranspiration at the catchment scale using satellite-based evapotranspiration data sets. *Water Resour. Res.* **47**, 9 (2011).
91. Weatherhead, E. K. & Howden, N. J. K. The relationship between land use and surface water resources in the UK. *Land Use Policy* **26**, S243–S250 (2009).
92. Stephens, W., Hess, T. M. & Knox, J. W. *Review of the Effects of Energy Crops on Hydrology*. https://dspace.lib.cranfield.ac.uk/handle/1826/3368 (2001).
93. Hunt, A. G., Sahimi, M. & Ghanbarian, B. Predicting streamflow elasticity based on percolation theory and ecological optimality. *AGU Adv.* **4**, e2022AV000867 (2023).
94. Greve, P., Roderick, M. L., Ukkola, A. M. & Wada, Y. The aridity Index under global warming. *Environ. Res. Lett.* **14**, 124006 (2019).
95. Zheng, Y., Coxon, G., Woods, R., Li, J. & Feng, P. Controls on the spatial and temporal patterns of rainfall-runoff event characteristics —a large sample of catchments across great Britain. *Water Resour. Res.* **59**, e2022WR033226 (2023).
96. Lee, L. J. E., Lawrence, D. S. L. & Price, M. Analysis of water-level response to rainfall and implications for recharge pathways in the Chalk aquifer, SE England. *J. Hydrol.* **330**, 604–620 (2006).
97. Hughes, A. G. et al. Flood risk from groundwater: examples from a Chalk catchment in southern England. *J. Flood Risk Manag.* **4**, 143–155 (2011).
98. Harrigan, S., Murphy, C., Hall, J., Wilby, R. L. & Sweeney, J. Attribution of detected changes in streamflow using multiple working hypotheses. *Hydrol. Earth Syst. Sci.* **18**, 1935–1952 (2014).
99. King, K. W., Fausey, N. R. & Williams, M. R. Effect of subsurface drainage on streamflow in an agricultural headwater watershed. *J. Hydrol.* **519**, 438–445 (2014).
100. Robinson, M. & Rycroft, D. W. The impact of drainage on streamflow. In *Agricultural Drainage* 767–800 (John Wiley & Sons, Ltd, 1999). https://doi.org/10.2134/agronmonogr38.c23.
101. Addor, N., Newman, A. J., Mizukami, N. & Clark, M. P. The CAMELS data set: catchment attributes and meteorology for large-sample studies. *Hydrol. Earth Syst. Sci.* **21**, 5293–5313 (2017).
102. Newman, A. J. et al. Development of a large-sample watershed-scale hydrometeorological data set for the contiguous USA: data set characteristics and assessment of regional variability in hydrologic model performance. *Hydrol. Earth Syst. Sci.* **19**, 209–223 (2015).
103. Lins, H. F. USGS hydro-climatic data network 2009 (HCDN-2009). https://pubs.usgs.gov/fs/2012/3047/ (2009).
104. Ramankutty, N., Evan, A. T., Monfreda, C. & Foley, J. A. Farming the planet: 1. Geographic distribution of global agricultural lands in the year 2000. *Glob. Biogeochem. Cycle* **22**, 1 (2008).
105. Coxon, G. et al. CAMELS-GB: hydrometeorological time series and landscape attributes for 671 catchments in Great Britain. *Earth Syst. Sci. Data* **12**, 2459–2483 (2020).
106. Robinson, E. L. et al. Climate hydrology and ecology research support system potential evapotranspiration dataset for Great Britain (1961-2015) [CHESS-PE]. *NERC Environ. Inf. Data Cent*. https://doi.org/10.5285/8baf805d-39ce-4dac-b224-c926ada353b7 (2016).
107. Bates, B., Kundzewicz, Z. & Wu, S. *Climate Change and Water*. (Intergovernmental Panel on Climate Change Secretariat, 2008).
108. Blöschl, G., Sivapalan, M., Wagener, T., Viglione, A. & Savenije, H. *Runoff Prediction in Ungauged Basins: Synthesis across Processes, Places and Scales*. (Cambridge University Press, 2013).
109. Greve, P. et al. Global assessment of trends in wetting and drying over land. *Nat. Geosci.* **7**, 716–721 (2014).
110. Greve, P. & Seneviratne, S. I. Assessment of future changes in water availability and aridity. *Geophys. Res. Lett.* **42**, 5493–5499 (2015).
111. Sherwood, S. & Fu, Q. A drier future? *Science* **343**, 737–739 (2014).
112. Zaerpour, M., Hatami, S., Sadri, J. & Nazemi, A. A global algorithm for identifying changing streamflow regimes: application to Canadian natural streams (1966–2010). *Hydrol. Earth Syst. Sci.* **25**, 5193–5217 (2021).
113. Xue, L. et al. Identification of potential impacts of climate change and anthropogenic activities on streamflow alterations in the Tarim River Basin, China. *Sci. Rep.* **7**, 8254 (2017).
114. Ketchum, D., Hoylman, Z. H., Huntington, J., Brinkerhoff, D. & Jencso, K. G. Irrigation intensification impacts sustainability of streamflow in the Western United States. *Commun. Earth Environ.* **4**, 1–8 (2023).
115. Fu, J. & Wang, W. On the lower bound of Budyko curve: the influence of precipitation seasonality. *J. Hydrol.* **570**, 292–303 (2019).
116. Nasta, P., Allocca, C., Deidda, R. & Romano, N. Assessing the impact of seasonal-rainfall anomalies on catchment-scale water balance components. *Hydrol. Earth Syst. Sci.* **24**, 3211–3227 (2020).
117. Merz, B., Vorogushyn, S., Uhlemann, S., Delgado, J. & Hundecha, Y. HESS Opinions 'More efforts and scientific rigour are needed to attribute trends in flood time series'. *Hydrol. Earth Syst. Sci.* **16**, 1379–1387 (2012).
118. Runge, J. Causal network reconstruction from time series: from theoretical assumptions to practical estimation. *Chaos* **28**, 075310 (2018).
119. Runge, J., Heitzig, J., Petoukhov, V. & Kurths, J. Escaping the curse of dimensionality in estimating multivariate transfer entropy. *Phys. Rev. Lett.* **108**, 258701 (2012).
120. Mosedale, T. J., Stephenson, D. B., Collins, M. & Mills, T. C. Granger causality of coupled climate processes: ocean feedback on the North Atlantic Oscillation. *J. Clim.* **19**, 1182–1194 (2006).
121. Spirtes, P., Glymour, C. N., Scheines, R. & Heckerman, D. *Causation, Prediction, and Search*. (MIT Press, 2000).
122. Spirtes, P. & Glymour, C. An algorithm for fast recovery of sparse causal graphs. *Soc. Sci. Comput. Rev.* **9**, 62–72 (1991).
123. Reichenbach, H. *The Direction of Time*. (University of California Press, 1991).
124. Ehret, U. et al. Advancing catchment hydrology to deal with predictions under change. *Hydrol. Earth Syst. Sci.* **18**, 649–671 (2014).
125. Beyers, D. W. Causal inference in environmental impact studies. *J. N. Am. Benthol. Soc.* **17**, 367–373 (1998).
126. Delforge, D., de Viron, O., Vanclooster, M., Van Camp, M. & Watlet, A. Detecting hydrological connectivity using causal inference from time series: synthetic and real karstic case studies. *Hydrol. Earth Syst. Sci.* **26**, 2181–2199 (2022).
127. Lee, S. & Ajami, H. Comprehensive assessment of baseflow responses to long-term meteorological droughts across the United States. *J. Hydrol.* **626**, 130256 (2023).

Acknowledgements

We gratefully acknowledge the financial support provided by the Natural Sciences and Engineering Research Council of Canada (NSERC Discovery Grant: RGPIN-2019-06894). We also thank Dr. Alireza Bahadori, Associate Editor, and Dr. Patricia Spellman, Editorial Board Member, for handling our manuscript. Finally, we sincerely appreciate the detailed and constructive comments from the three anonymous reviewers, which have greatly enhanced this paper.

Author contributions

M.Z., S.H., W.K., S.P., A.P., and M.C. conceived the motivation and designed the study. M.Z. and A.B. collected data. M.Z. performed the analysis; M.Z., S.H., and A.B. drafted the paper and prepared figures. All authors contributed to the writing, reviewing, and interpretation of the results and to the text.

Competing interests

The authors declare no competing interests.

Additional information

Supplementary information The online version contains supplementary material available at https://doi.org/10.1038/s43247-024-01891-w.

Correspondence and requests for materials should be addressed to Masoud Zaerpour.

Peer review information *Communications Earth & Environment* thanks Fernando Jaramillo and the other, anonymous, reviewer(s) for their contribution to the peer review of this work. Primary Handling Editors: Patricia Spellman and Alireza Bahadori. A peer review file is available.